EROSION RATE DIAGNOSTICS IN ION THRUSTERS USING LASER-INDUCED FLUORESCENCE*

C. J. Gaeta,** R. S. Turley,** J. N. Matossian,†
J. R. Beattie,‡ W. S. Williamson,†† and J. D. Williams†
Hughes Research Laboratories, Malibu, CA 90265

ABSTRACT

We have demonstrated the use of laser-induced fluorescence (LIF) to monitor the charge-exchange ion erosion of the molybdenum accelerator electrode in ion thrusters. This real-time, nonintrusive method was implemented by operating a 30-cm-diameter ring-cusp thruster using xenon propellant. With the thruster operating at a total power of 5 kW, laser radiation at a wavelength of 390 nm (corresponding to a ground state atomic transition of molybdenum) was directed through the extracted ion beam adjacent to the downstream surface of the molybdenum accelerator electrode. Molybdenum atoms, sputtered from this surface as a result of charge-exchange ion erosion, were excited by the laser radiation. The intensity of the laser-induced fluoresence radiation, which is proportional to the sputter rate of the molybdenum atoms, was measured and correlated with variations in thruster operating conditions such as accelerator electrode voltage, accelerator electrode current, and test facility background pressure.

NOMENCLATURE

A_{ij}	=	Einstein A coefficient between levels i and j, sec^{-1}
a_o	=	Bohr radius, m
c	=	speed of light in free space, m/sec
e	=	charge of the electron, C
f_{ij}	=	atomic transition oscillator strength
g	=	linewidth distribution function, sec
$\bar{g}$	=	energy-averaged Gaunt factor
g_i	=	degeneracy for atomic level i
h	=	Planck's constant, J·sec
$\hbar$	=	Planck's constant/2π, J·sec
I	=	intensity of optical radiation, W/m^2
J_A	=	accelerator electrode current, A
J_b	=	extracted beam ion current, A
J_E	=	cathode emission current, A
k	=	Boltzmann's constant, J/°K
M_A	=	mass of molybdenum atom, kg
m_e	=	mass of the electron, kg
n_e	=	Maxwellian electron density in the extracted beam, m^{-3}
P_b	=	beam power, W
P_o	=	vacuum chamber pressure, Pa
P_T	=	total thruster power, W
R_p	=	electron-impact excitation rate, m^3/sec
R_{re}	=	atomic stimulated excitation rate, m^3/sec
R_∞	=	Rydberg energy, eV
kT_A	=	temperature of molybdenum atom, eV
kT_e	=	electron temperature, eV
V_A	=	accelerator electrode voltage, V
V_B	=	beam voltage, V
V_D	=	discharge voltage, V
Y	=	sputter yield, atoms/ion
ϵ_i	=	beam-ion-production cost, W/A
ϵ_o	=	permittivity of free space, F/m
λ	=	wavelength of optical radiation, m
η_e	=	electrical efficiency, %
$(\eta_{md})_{unc}$	=	discharge propellant utilization efficiency (uncorrected for doubly charged ions), %
χ_{ij}	=	energy difference between levels i and j, eV

*This work was supported by NASA under contract number NAS 3-25553

**Member of the Technical Staff, Optical Physics Department
†Member of the Technical Staff, Plasma Physics Department, Member AIAA
‡Project Manager, Plasma Physics Department, Senior Member AIAA
††Senior Staff Physicist, Plasma Physics Department, Member AIAA

INTRODUCTION

The inherent low-thrust capability of ion thrusters generally dictates long operating times ranging from 4000 to 10,000 hours,[1–4] depending upon thruster size and mission requirements. This, in turn, imposes a concomitant requirement on the lifetime of thruster components.

It is generally regarded that the primary lifetime-limiting wear mechanism in xenon ion thrusters is charge-exchange ion erosion of the molybdenum accelerator electrode.[5,6] This wear process has been found to be far more significant than ion erosion of the cathode and the cathode-potential screen electrode[6], as well as the anode potential surfaces of the discharge chamber. Due to the interest in near-term applications of high power (5 kW) xenon ion thrusters, such as space vehicle orbit raising, an accurate, real-time measurement of the wear rate of the accelerator electrode is critical to providing an assessment of thruster performance and lifetime.

One method of measuring the wear rate of the accelerator electrode relies on the use of laminar thin-film badges.[7] However, this technique typically requires tests of long duration (~ tens of hours) to provide an accurate assessment of component lifetime. This can restrict the quantity of test data and does not provide a real-time correlation between component wear rate, thruster operating parameters, and thruster performance.

Optical methods offer the potential of providing such a real-time data acquisition and wear rate evaluation. Optical emission spectroscopy[8] has been used to correlate measured optical emission intensity of excited sputtered molybdenum atoms with electrode wear rate. However, its use relies upon simultaneous measurements of discharge chamber plasma properties, such as electron temperature and density, as well as the solution of a system of simultaneous equations by numerical techniques to yield the wear rate. This results in an indirect assessment of the wear rate and does not occur in real-time.

We have developed and demonstrated an alternative optical diagnostic method, based on laser-induced fluorescence (LIF),[9–14] which circumvents these limitations to provide a real-time monitor of the wear rate of the molybdenum accelerator electrode in ion thrusters. This method also facilitates the correlation of accelerator electrode wear with changes in thruster performance.

The LIF technique was demonstrated by operating a 30-cm-diameter ring-cusp ion thruster with xenon propellant at a nominal 5-kW power level. Charge-exchange ion erosion of the accelerator electrode resulted in a flux of molybdenum atoms downstream of the electrode. Fluorescence of the sputtered atoms was induced by an optical field from a continuous wave dye laser operating in the ultraviolet at a wavelength corresponding to a ground state transition of molybdenum. The fluorescence level, which is proportional to the density of the sputtered atoms, was correlated with variations in accelerator electrode voltage, test facility background pressure, and discharge chamber operating conditions. Although this technique has been developed specifically for ion thrusters, it is applicable to any system involving the erosion of a surface immersed in a plasma or subject to ion beam bombardment. In particular, the laser-induced fluorescence technique should provide a real-time diagnostic of cathode erosion experienced in other electric propulsion devices such as magnetoplasmadynamic (MPD) and arcjet thrusters.[15–16]

Laser-induced fluorescence is intrinsically nonintrusive and has the potential for providing high spatial resolution, real-time monitoring of the density of atomic species anywhere within a volume of interest. In addition, it can also determine the atomic state of the species.[9,10] For example, LIF has been used to determine particle densities in reactive plasmas.[14] Laser-induced fluorescence has also been used as a tool for the study of surfaces eroded by directed ion beams,[11–13] as well as surfaces immersed in a plasma.[17] In the following sections we present theoretical background and experimental results which validate the use of the laser-induced fluorescence technique as a wear rate diagnostic in ion thrusters.

THEORETICAL BACKGROUND

In laser-induced fluorescence, atoms are stimulated by an external resonant laser source, in addition to the inherent stimulation by the electrons in the plasma. The LIF signal is independent of the plasma conditions, provided the plasma does not significantly affect the density of the ground state atoms. We selected the ground state atomic transition process ($\lambda = 390.2$ nm) for molybdenum atoms that provided the largest fluorescence signal for a given laser power.

Plasmas produced in ion thruster discharge chambers are characterized as partially ionized ~ 10%, low pressure ~ 10^{-3}–10^{-2} Pa (10^{-5}–10^{-4} Torr) plasmas with an average electron temperature of 2–5 eV. Discharge chamber plasma densities are on the order of 10^{10}–$10^{11}/cm^3$,[18,19] while beam plasma densities are on the order of $10^9/cm^3$. For the beam plasma

parameters, less than 1% of the molybdenum atoms sputtered from a surface exposed to the plasma are raised to excited states as a result of collisions with electrons.[8] In order to achieve a high signal-to-noise ratio (large ratio of the laser-induced to collision-induced signals) in the laser-induced fluorescence method, the excitation of molybdenum atoms must be dominated by laser photon absorption. Therefore, we must determine the ratio of laser-induced to collision-induced excitation rates of molybdenum atoms as a function of laser intensity.

The contributions of collisional ionization, three-body recombination, radiative recombination, dielectronic recombination, and absorption are negligible for plasmas,[20] such as those found in ion thruster discharge chambers and the extracted beam. Therefore, we neglect these contributions in the theoretical development described below. More detailed quantum mechanical treatments of laser-induced fluorescence are available in the literature.[21]

The rate for atomic stimulated excitation, R_{re}, is given in terms of the Einstein A coefficient as[22]

$$R_{re}(i \rightarrow j) = \frac{g_j}{g_i} \frac{\pi \hbar^2 c^2 I A_{ji} g}{2 \chi_{ij}^3}, \tag{1}$$

where g_i and g_j are the degeneracies for atomic levels i and j, respectively, I is the intensity of the radiation, A_{ji} is the Einstein A coefficient, and χ_{ij} is the energy difference between levels i and j. The Doppler distribution function g, evaluated at line center of the transition, is given by[23]

$$g = \frac{h}{\chi_{ij}} \sqrt{\frac{M_A c^2}{2 \pi k T_A}}, \tag{2}$$

where k is Boltzmann's constant, M_A and T_A are the mass and temperature of the molybdenum atom, respectively, and h is Planck's constant. Since the energy distribution of sputtered atoms from a surface subjected to ion bombardment is $\sim$ 1–2% of the incident ion energy,[24] $kT_A \sim 1$ eV for the conditions of our experiment.

A semi-empirical formula for the electron-impact (collision-induced) excitation rate between states i and j, $R_p(i \rightarrow j)$, is[25]

$$R_p(i \rightarrow j) = 16 \sqrt{\frac{2\pi}{3 m_e}} \frac{f_{ij} \bar{g} \pi a_0^2 n_e R_\infty^2}{\sqrt{k T_e}\, \chi_{ij}} \exp\left(-\frac{\chi_{ij}}{k T_e}\right), \tag{3}$$

where m_e is the electron mass, R_∞ is the Rydberg energy (13.51 eV), T_e is the electron temperature, f_{ij} is the oscillator strength for the transition from level i to level j, $\bar{g}$ is the energy-averaged Gaunt factor (a correction factor), a_0 is the Bohr radius, and n_e is the electron density in the extracted beam. Under our operating conditions $\bar{g}$ is assumed to be unity. The use of Equation (3) assumes that the electron energies can be characterized by a (local) Maxwellian energy distribution which has been shown to adequately describe the electrons in the extracted ion beam.[26]

Equation (3) can be cast into a form that allows for a more convenient comparison to radiative excitation by relating the oscillator strength to the Einstein A coefficient by[22]

$$f_{ij} = \frac{4 \pi \epsilon_o m_e c^3 \hbar^2 g_j A_{ji}}{2 e^2 g_i \chi_{ij}^2}. \tag{4}$$

In terms of fundamental constants and the spontaneous decay from the excited state, the plasma excitation rate is given by

$$R_p(i \rightarrow j) = 2 \sqrt{\frac{2 \pi^3 m_e c^2}{3 k T_e}} \frac{\hbar^2 c^2 e^2 g_j A_{ji} n_e}{4 \pi \epsilon_o \chi_{ij}^3 g_i} \exp\left(-\frac{\chi_{ij}}{k T_e}\right). \tag{5}$$

Assuming that the decay processes and rates are the same for atoms excited by either plasma electrons or optical photons, the relative intensity of the LIF signal compared to the background (plasma-induced) flourescence signal is given by the ratio of the excitation rates for the two processes.

$$\frac{R_{re}}{R_p} = \frac{4 \pi \epsilon_o I g}{e^2 n_e} \sqrt{\frac{3 k T_e}{2 \pi m_e c^2}} \exp\left(\frac{\chi_{ij}}{k T_e}\right) \tag{6}$$

The appropriate value of g to use is given by Equation (2). Assuming $kT_A = 1$ eV and $2\pi\hbar c/\chi_{ij} = 390.2$ nm yields $g = 1.55 \times 10^{-10}$ sec. In our experiments, we used an ultraviolet beam from a Coherent 599 dye laser with an intensity of approximately 100 W/m^2 inside the vacuum test facility. Equation (6) can then be evaluated using the parameters $n_e = 6 \times 10^{15}$ m^{-3}, $kT_e = 3$ eV, and $\chi_{ij} = 3.18$ eV. This gives a value of 54 for the ratio R_{re}/R_p, which is large enough to provide ample signal for determining the molybdenum density when phase-sensitive detection techniques are employed.

This calculation applies to the same volume of atoms for both excitation modes (plasma and radiative). In practice, the geometry of the measurement is very important and it is difficult to completely isolate the volume of atoms intercepted by the laser beam to avoid fluorescence contributions

from other regions where the excitation mechanism is solely collisional. Although shielding was used in the experiment to minimize this additional contribution, a plasma background signal was still present. Therefore, a phase-sensitive detection technique, described in the experimental sections, was employed and achieved a high signal-to-noise ratio. However, it was still necessary to keep the background fluorescence contribution small in order to avoid saturation of the detector.

Commercially available Ti:Sapphire lasers are much easier to maintain than a dye laser system and would probably be selected as the optical source in a practical diagnostic station. Using internal cavity doubling, these lasers can produce 200 mW of output power at 390 nm, which is resonant with the lowest lying dipole-allowed molybdenum ground state transition. If this beam is collimated to a 1 cm^2 spot, the intensity, I, would be 2000 W/m^2. This gives a value for R_{re}/R_p of 1800 for the Ti:Sapphire laser, which should produce a very good signal-to-noise ratio.

We have performed experiments, described in the following sections, using a dye laser system. The results of these experiments validate the conclusions of the simple physical model presented above.

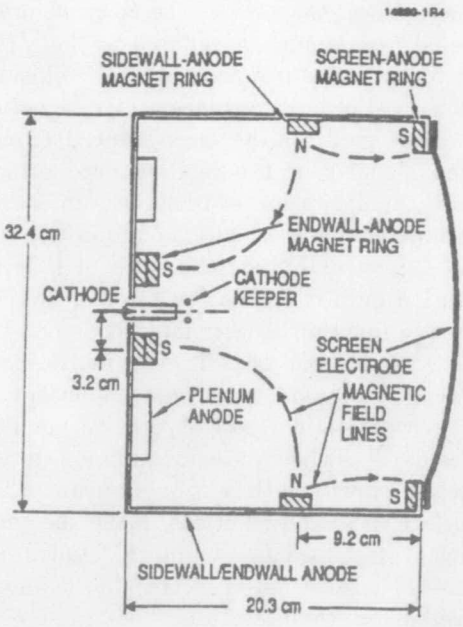

Figure 1. Schematic diagram of a 30-cm-diameter ring-cusp ion thruster.

EXPERIMENTAL SETUP

Figure 1 shows a schematic diagram of the 30-cm-diameter ring-cusp ion thruster used in the LIF experiment. A detailed description of the design and operating characteristics of this thruster are available in the literature.[19,27] To demonstrate the LIF technique, the thruster was operated with a two-grid ion extraction assembly consisting of screen and accelerator electrodes.

The vacuum test facility employed is illustrated in Figure 2. It is a 3-meter-diameter, 6-meter-long chamber which is cryopumped and has a pumping speed of 135,000 liters/sec for xenon. The baseline pressure in the facility is 4×10^{-6} Pa (3×10^{-8} Torr).

Several features were incorporated in order to adapt the vacuum chamber to facilitate demonstration of the LIF technique. As shown in Figure 2, collimators were employed to minimize the contribution of laser light scattered from surfaces within the vacuum chamber. One such collimator extended from the output side port into the vacuum chamber approximately 0.5 m to minimize the contribution of reflected laser light. Another was placed at the laser beam input port, located on top of the vacuum test facility, and extended approximately the same distance into the vacuum chamber. A curved quartz horn, coated with black soot from an acetylene torch, was installed at the bottom of the chamber (within another collimator) to terminate propagation of the laser light with minimum optical scattering.

Figure 3 shows a photograph of the LIF experimental setup. This arrangement employs a continuous-wave laser source consisting of a Coherent I-18 argon ion laser operating in the 350–360 nm spectral range and a Coherent 599 standing-wave tuneable dye laser capable of emitting radiation at the relevant molybdenum resonance (λ = 390 nm). The argon laser serves as an optical pump source for the dye laser. Coarse frequency tuning of the dye laser is accomplished with an intracavity birefringent plate which serves as a low loss element (Brewster angle plate) for a narrow range of frequency ($\sim$ 200 GHz). The absolute position of this frequency passband is adjusted by rotation of the tuning element. Etalons are also available for use within the laser cavity to spectrally narrow the laser emission to a single frequency with a jitter of less than 20 MHz. However, we determined that the birefringent tuning plate sufficiently narrowed the spectrum of the laser emission for the purpose of our experiment (because of Doppler broadening of the atomic transition), and the etalons were not employed.

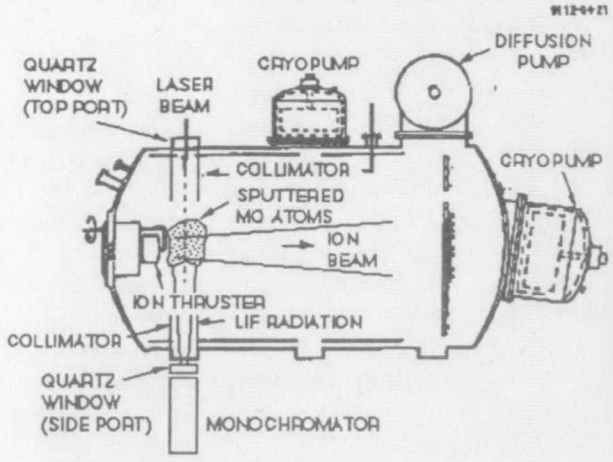

Figure 2. Schematic diagram of the vacuum chamber test facility.

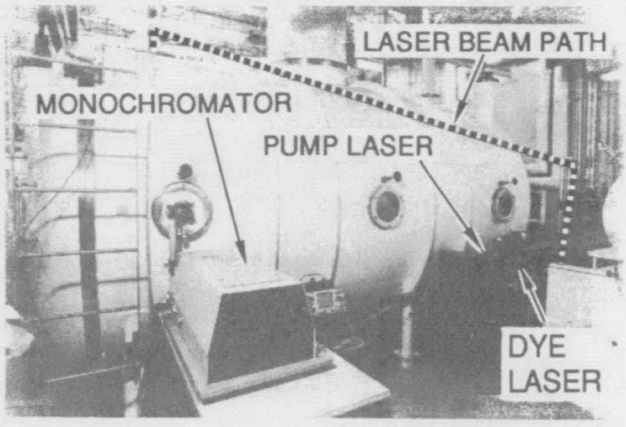

Figure 3. Illustrated photograph showing the experimental arrangement for laser-induced flourescence measurements.

A beamsplitter directed a small portion of the output from the dye laser into a power meter in order to monitor the output power of the laser. The majority of the dye laser output was directed through the top port of the vacuum chamber using an arrangement of mirrors, as shown in Figure 3. The laser beam then propagated through a region containing molybdenum atoms sputtered from the accelerator electrode of the ion thruster. Figure 4 (which was taken from the open end of the vacuum test chamber) shows the top port and collimator through which the laser beam enters the chamber. The collimator housing the quartz horn, which absorbs the laser radiation, is shown at the bottom of the vacuum chamber. A collimator that minimizes scattered light reaching the monchromator is visible in the right of the photo.

A movable molybdenum plate functioned as a reflector to allow laser light, or plasma-induced fluorescence from within the discharge chamber, to reach the monochromator for calibration purposes. The molybdenum plate also served as a strong source of sputtered material which was used for initial adjustment of both the laser frequency and the monochromator wavelength.

In order to discriminate against other spectral lines, a portion of the laser-induced fluorescence was collected with a 60-cm focal length lens, directed into a Spex model 1700-11 monochromator ($\sim$ 0.03 nm resolution), and detected with a photomultiplier tube. The focal length of the collection lens was chosen to provide a close match to the f-number of the monochromator. This procedure filled the diffraction grating in the monochromator, allowing the best spectral resolution to be realized, depending upon the width of the entrance and exit slits. These slits were wide open for our experiments ($\sim$ 2 mm), but this mode of operation did not adversely affect the signal to noise ratio.

It should be noted that the present experimental setup does not allow for three dimensional spatial resolution within the molybdenum flux. This type of resolution could be achieved by overlapping multiple laser beams in conjunction with a threshold detector. An alternative technique for accomplishing this type of resolution involves a single laser beam and a double pinhole arrangement at the detector port. One could also employ spatial filtering techniques at the light collection aperture.

We further note that the LIF technique may be extended to provide for simultaneous measurement of the erosion rates of multiple surfaces constructed with different materials. For example, to concurrently measure the erosion of the tungsten orifice plate of the hollow cathode, another laser source, operating at the appropriate wavelength, would be combined with the dye laser mentioned in our current experiment. A beamsplitter at the output port would then direct the output fluorescence into two separate detectors, each equipped with spectral filters, allowing selective measurement of the two fluorescence wavelengths. In a situation where all surfaces are comprised of the same material, such as molybdenum, the relative contributions to the fluorescence signal must be assessed as part of the calibration process.

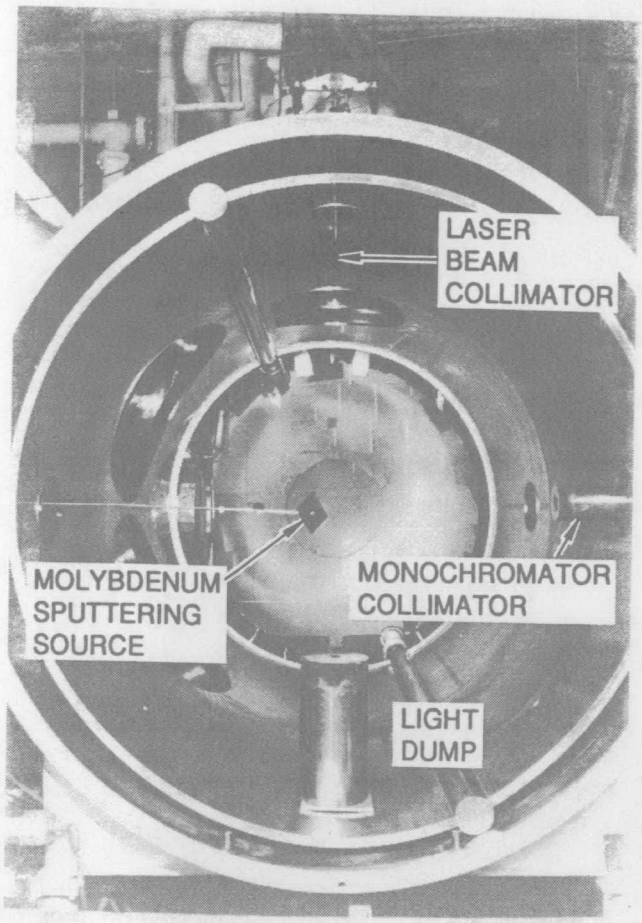

Figure 4. Photograph of the interior of the vacuum chamber test facility.

LIF EXPERIMENTS AND RESULTS

Prior to implementing the laser-induced fluorescence technique for measuring the charge-exchange ion erosion of the accelerator electrode in an operating ion thruster, we conducted a separate series of experiments to optimize the laser and detection system parameters.[17] In these earlier tests, we operated a discharge chamber (with the ion extraction assembly removed) and simulated the accelerator electrode with a molybdenum foil. This foil could be biased at potentials similar to those of an accelerator electrode ($\sim$ 100–300 volts). We adapted this procedure for use in the experimental work described in this paper.

The output from the dye laser was set to a wavelength corresponding to the desired molybdenum resonance ($\lambda = 390.2$ nm) using the intracavity birefringent tuning element. The laser output power during the experiment was approximately 5 mW, while the intensity within the vacuum chamber was about 100 W/m^2.

In order to further reduce the contribution from the plasma-induced fluorescence, the laser beam was amplitude modulated with a chopper at a frequency of 1 kHz. This resulted in a modulation of the LIF signal at the same frequency, in contrast to the relatively constant level of the plasma-induced background. A lock-in amplifier was then used to eliminate the dc background due to the plasma excitation. Both the dc-coupled output from the photomultiplier tube and the output from the lock-in amplifier were observed simultaneously on a dual trace oscilloscope and a strip chart recorder.

The radiation exiting the monochromator was comprised of the LIF and plasma-induced fluorescence (PIF) contributions, in addition to scattered laser light. As shown in Figure 2, the monochromator did not have a direct line-of-sight view of the discharge chamber plasma. Although this geometry is desireable from a signal-to-noise standpoint it makes it more difficult to set parameters such as the laser frequency and alignment of the detection system. This was accomplished using the movable molybdenum plate mentioned in the previous section. Initial alignment of the mirrors, lens and monochromator was performed by extending the plate into the flux of extracted ions so that a large plasma-induced fluorescence signal was obtained. With the plate immersed in the ion beam in this manner a copious source of sputtered molybdenum atoms was generated. When the laser beam traversed this high density region a strong laser-induced fluorescence signal was detected, allowing for optimization of the laser wavelength and detection system parameters. Once this was accomplished, the plate was retracted and the experiments were conducted.

We operated the thruster at a nominal 5-kW power level. The nominal operating parameters at this power level are summarized in Table 1. Figure 5 shows LIF signal measurements (the output of the photomultiplier tube was normalized by the measured laser output power, which drifts slightly) as a function of accelerator electrode current for two different accelerator voltages. The accelerator current was increased by introducing xenon into the vacuum chamber from an auxiliary gas source. The data shown in the figure illustrate a linear dependence of the LIF signal (molybdenum erosion rate) with accelerator electrode current for two levels of the accelerator voltage. In addition, there is an increase in the LIF signal level with accelerator electrode volt-

Table 1: Thruster Operating Parameters

Discharge Voltage V_D (V)	28
Cathode Emission Current J_E (A)	14
Beam-Ion-Production Cost ϵ_i (eV/ion)	129
Extracted Beam Ion Current J_b (A)	3
Beam Voltage V_B (V)	1500
Accelerator Electrode Voltage V_A (V)	350
Accelerator Electrode Current J_A (mA)	23
Beam Power P_b (W)	4560
Total Thruster Power P_T (W)	5024
Electrical Efficiency η_e (%)	90
Propellant Utilization $(\eta_{md})_{unc}$ (%)	86

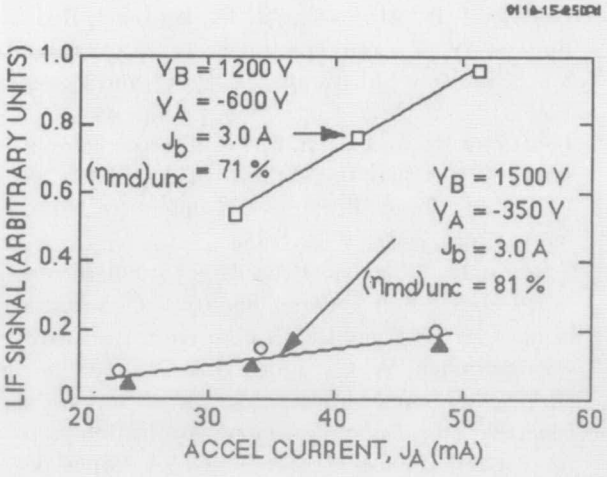

Figure 5. Variation of the laser-induced fluorescence signal as a function of accelerator current.

age. This behavior can be understood on the basis of simple physical arguments.[27]

The total accelerator electrode current is comprised of two parts:[26] charge-exchange current and direct-ion interception. Direct-ion interception is independent of the neutral gas density and depends soley upon the geometry and alignment of the ion extraction assembly apertures. The charge-exchange current, however, is proportional to the product of the beam current and the neutral density. For constant beam current, the charge-exchange current (and therefore the total accelerator electrode current) increases linearly with the neutral density. By introducing xenon gas into the vacuum chamber, there should be a linear increase in the density of molybdenum atoms sputtered from the electrode. The linear variation of the LIF signal with accelerator electrode

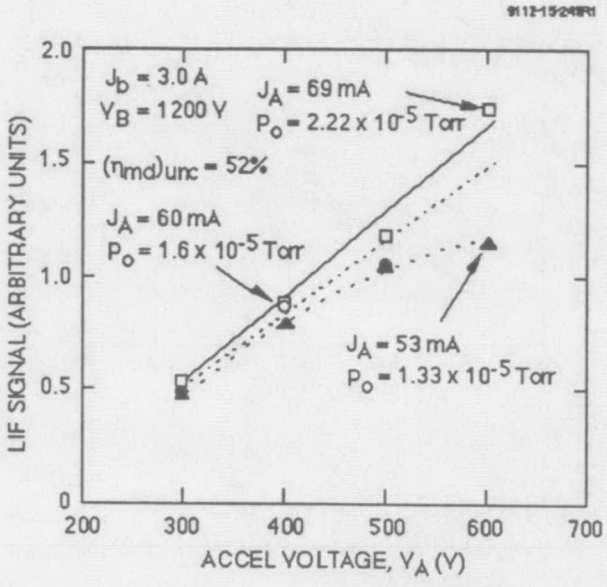

Figure 6. Variation of the laser-induced fluorescence signal with accelerator voltage.

current shown in Figure 5 is consistent with this behavior. Furthermore, the relative increase in the LIF signal with accelerator voltage, also shown in the figure, is consistent with an increase in sputter yield caused by an increase in ion energy.

We further explored the dependence of the LIF signal level with accelerator voltage. Figure 6 shows the variation of the LIF signal as a function of accelerator voltage for constant beam current. For each of the three curves the pressure in the chamber was maintained constant at the indicated values. At a constant accelerator voltage level (i.e., $V_A = -600$ V) the LIF signal increases with increasing pressure. Similarly, for constant pressure, i.e. $P_o = 1.8 \times 10^{-3}$ Pa (1.3×10^{-5} Torr), the LIF signal increases with accelerator voltage. This behavior is also consistent with the simple physical model mentioned above. For example, at constant pressure the charge-exchange ion current should also be constant. Increasing the accelerator voltage results in an increased ion energy and sputtering rate, yielding an increase in the LIF signal, as shown in the figure. Alternatively, for constant accelerator voltage (constant ion energy), an increase in chamber pressure will result in an increased charge-exchange ion current, producing a larger LIF signal.

To gain additional physical insight from the data shown in Figure 6, we plotted the variation of sputter yield[28] with accelerator voltage in Figure 7 for one of the curves from Figure 6. The data indicate that

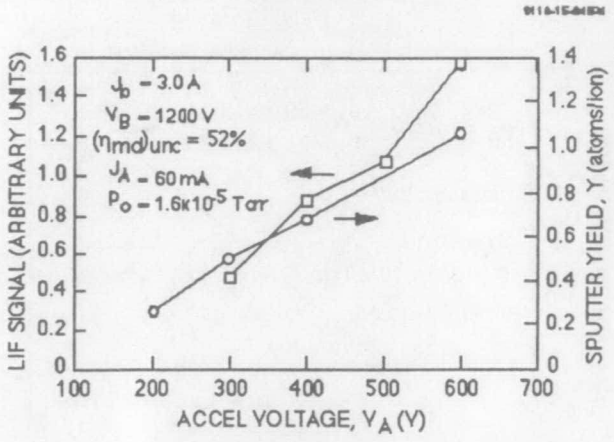

Figure 7. Comparison of LIF signal level and sputter yield behavior as a function of accelerator voltage level.

the LIF signal and the sputter yield have the same functional dependence on accelerator voltage.

On the basis of the experimental results presented in Figures 5, 6, and 7 we believe that laser-induced fluorescence can be used as a real-time diagnostic for assessing relative accelerator grid wear rates in ion thrusters. Absolute wear rates should be obtainable by calibrating the LIF signal with actual measured wear rates.

CONCLUSION

We have demonstrated of the use of laser-induced fluorescence for dynamically measuring the charge-exchange ion erosion of the molybdenum accelerator electrode in xenon ion thrusters. This technique has been demonstrated at a nominal 5-kW operating power level for the thruster. The LIF signal showed excellent correlation with variations in thruster operating conditions such as accelerator electrode voltage, accelerator electrode current, and test facility background pressure.

The LIF method is a real-time, nonintrusive diagnostic tool which should aid in optimizing and evaluating thruster performance characteristics, as well as providing an assessment of thruster component lifetime without having to cycle through the lengthy operating times required of conventional diagnostics, such as laminar thin-film erosion badges. This technique should be widely applicable to other electric propulsion devices, such as MPD and arcjet thrusters.

ACKNOWLEDGEMENT

The authors are grateful to Dr. Ross McFarlane, Mr. Jim Brown and Mr. Robert Cronkite for the use of the lasers, as well as Coherent, Inc. for assistance on laser operation at ultraviolet wavelengths. They also thank Mr. Ray Maheux and Mr. Gunter Fehlhauer for design and fabrication of the plasma source, as well as Mr. Alan Ward for work on adapting the vacuum test facility for the LIF measurements.

REFERENCES

1. Beattie, J. R., Matossian, J. N., Poeschel, R. L., Rogers, W. P., and Martinelli, R. M., "Xenon Ion Propulsion Subsystem," J. Prop. and Power, Vol. 5, No. 4, July–Aug. 1989, pp.438–444.
2. Beattie, J. R. and Penn, J. P., "Electric Propulsion - A National Capability," AIAA Paper 89-2490, 25th Joint Propulsion Conference, Monterey, Calif., July 10–12, 1989.
3. Schreib, R., "Electric Propulsion: Implementation Issues," AIAA Paper 88-006, 20th International Electric Propulsion Conference, Garmisch-Partenkirchen, W. Germany, Oct. 3–6, 1988.
4. Birkan, M. and Micci, M. M., "Survey of Electric Propulsion Thruster Applicability to Near Earth Space Missions," AIAA Paper 88-065, 20th International Electric Propulsion Conference, Garmisch-Partenkirchen, W. Germany, Oct. 3–6, 1988.
5. Beattie, J. R. and Matossian, J. N., "Xenon Ion Propulsion for Stationkeeping and Orbit Raising," Paper IEPC-88-052, 20th International Electric Propulsion Conference, Garmisch-Partenkirchen, W. Germany, Oct. 3–6, 1988.
6. Beattie, J. R., Matossian, J. N., and Robson, R. R., "Status of Xenon Ion Propulsion Technology," J. Prop. and Power, Vol. 6, No. 2, March–April 1990, pp. 145–150.
7. Beattie, J. R., "A Model for Predicting the Wearout Lifetime of the LeRC/Hughes 30 cm Mercury Ion Thruster," AIAA Paper No. 79-2079, 14th International Electric Propulsion Conference, Princeton, New Jersey, Oct. 30 – Nov. 1, 1979.
8. Rock, B. A., Mantenieks, M. A., and Parsons, M. L., "Rapid Evaluation of Ion Thruster Lifetime Using Optical Emission Spectroscopy," AIAA Paper No. 85-2011, 18th International Electric Propulsion Conference, Alexandria, Virginia,

Sept. 30 – Oct. 3, 1985.

9. Killinger, D. K., Wang, C. C., and Hanabusa, M., "Intensity and Pressure Dependence of Resonance Fluorescence of OH Induced by a Tunable UV Laser," Phys. Rev. A, Vol. 13, No. 6, June 1976, pp. 2145–2152.
10. Heidner III, R. F., Helvajian, H., Holloway, J. S., and Koffend, J. B., "Direct Observation of NF(X) Using Laser Induced Fluorescence: Determination of the $H + NF_2$ Branching Ratio," The Aerospace Corp. Report SSD-TR-90-28, Sept. 1990.
11. Calaway, W. F., Young, C. E., Pellin, M. J., and Gruen, D. M., "Laser-Induced Fluorescence as a Tool for the Study of Ion Beam Sputtering," in Handbook of Ion Beam Processing Technology, edited by J. J. Cuomo, S. M. Rossnagel and H. R. Kaufman, Noyes Publications, Park Ridge, New Jersey, 1989, pp. 112–127.
12. Bay, H. L., "Laser Induced Fluorescence as a Technique for Investigations of Sputtering Phenomena," Nuclear Instr. and Methods in Phys. Research B, Vol. 18, 1987, pp. 430–445.
13. Husinsky, W., "The Application of Doppler Shift Laser Fluorescence Spectroscopy for the Detection and Energy Analysis of Particles Evolving from Surfaces," J. Vac. Sci. Technol., Vol. B3, No. 5, Sept.–Oct. 1985, pp. 1546–1559.
14. Miller, T. A., "Optical Emission and Laser-Induced Fluorescence Diagnostics in Reactive Plasmas," J. Vac. Sci. Technol., Vol. A4, No. 3, May–June 1986, pp. 1768–1772.
15. Kurtz, H. L., Auweter-Kurtz, M., Glocker, B., Habiger, H., Merke, W., and Schrade, H. O., "Cylindrical Steady-State MPD Thruster," AIAA Paper No. 88-025, 20^{th} International Electric Propulsion Conference, Garmisch-Partenkirchen, W. Germany, Oct. 3–6, 1988.
16. Yoshikawa, T., Onoe, K., Yoshida, H., Kotani, S., Suzuki, H., and Uematsu, K., "Operating Characteristics of 1 kW Hydrazine Arcjet Thruster," AIAA Paper No. 88-108, 20^{th} International Electric Propulsion Conference, Garmisch-Partenkirchen, W. Germany, Oct. 3–6, 1988.
17. Gaeta, C. J., Turley, R. S., Matossian, J. N., Beattie, J. R., and Williamson, W. S., "Plasma Erosion Rate Diagnostics Using Laser-Induced Fluorescence," submitted to Rev. Scientific Instr., 1991.
18. Matossian, J. N. and Beattie, J. R., "Model for Computing Volume-Averaged Plasma Properties in Electron-Bombardment Ion Thrusters," J. Prop. and Power, Vol. 5, No. 2, March–April 1989, pp. 188–196.
19. Matossian, J. N. and Beattie, J. R., "Characteristics of Ring-Cusp Discharge Chambers," J. Prop. and Power, to be published Nov.–Dec. 1991.
20. Chapman, B., Glow Discharge Processes, John Wiley and Sons, New York, 1980.
21. Kimble, H. J. and Mandel, L., "Theory of Resonance Fluorescence," Phys. Rev. A, Vol. 13, No. 6, June 1976, pp. 2123–2143.
22. Stone, J. M., Radiation and Optics, McGraw-Hill, New York, 1963.
23. Yariv, A., Quantum Electronics,Second Edition, John Wiley and Sons, New York, 1975.
24. Kaminsky, M., Atomic and Ionic Impact Phenomena on Metal Surfaces, Academic Press, New York, 1965.
25. Whitney, K. G. and Davis, J., "Hot-Spot Model of K-Line Emission from Laser-Heated Plasmas," J. Appl. Phys., Vol. 45, No. 12, Dec. 1974, pp. 5294–5302.
26. Kaufman, H. R., in Advances in Electronics and Electron Physics, Vol. 36, Academic Press, New York, 1974, pp. 265–373.
27. Beattie, J. R. and Matossian, J. N., "High Power Ion Thruster Technology," Hughes Research Laboratories, Malibu, CA, NASA CR-187161, Nov. 1991.
28. Rosenberg, D. and Wehner, G. K., "Sputtering Yields for Low Energy He^+-, Kr^+-, and Xe^+-Ion Bombardment," J. Appl. Phys., Vol. 33, No. 5, May 1962, pp. 1842–1845.